Journal of Applied Fluid Mechanics, Vol. 15, No. 6, pp. 1759-1770, 2022.
Available online at www.jafmonline.net, ISSN 1735-3572, EISSN 1735-3645.
https://doi.org/10.47176/jafm.15.06.1153

Particle Dynamic Characteristics of the Vertical Tubes in a Horizontal-Vertical Pneumatic Conveying System with Different Curvature Radius Bends

F. Yan[1], Z. Y. Yang[1], P. P. Tu[1] and R. Zhu[2†]

[1] *School of Mechanical Engineering, Jiangsu University of Science and Technology, Jiangsu, Zhenjiang 212000, China*
[2] *School of Environmental and Chemical Engineering, Jiangsu University of Science and Technology, Jiangsu, Zhenjiang 212000, China*

†*Corresponding Author Email: zhurui@just.edu.cn*

(Received March 26, 2022; accepted July 6, 2022)

ABSTRACT

To examine the flow characteristics of particles in the vertical tube corresponding to different curvature radius bends, the particle velocity is measured at the Minimum Pressure Drop (MPD) using a high-speed Particle Image Velocimeter (PIV). This experiment explores the effects of particle flow characteristics at different curvature radius bends and their corresponding vertical tubes with pressure drop, power consumption, the intensity of particle fluctuation velocity, power spectrum and time-frequency characteristics. It is observed that the pressure drop and power consumption can be reduced with the help of a large curvature radius bend. Besides, the reduction of particle velocity in the large curvature radius bend and its corresponding vertical tube is less, and the particle possesses a larger intensity of fluctuation velocity in its corresponding vertical tube. The particles in the vertical tube corresponding to the large curvature radius bend lead to large peaks of the power spectrum in the low-frequency region, which is closely linked to the pressure drop. Eventually, the dynamics of particles in a vertical tube are revealed from the perspective of time-frequency analysis by using a continuous wavelet transform.

Keywords: Pneumatic conveying; Vertical tube; Particle fluctuating velocity; Power spectrum; Wavelet transform.

NOMENCLATURE

A_p	projected area of the particle	U_a	gas velocity
a	bulk voidage	ρ	particle density
D_r	pressure drop normalization factor	ρ_a	gas density
d_{ep}	equivalent diameter	μ	poisson ratio
E	power consumption coefficient	θ	included angle
G	shear elasticity	u_p	axial particle velocity
G_s	particle mass flow rate	ω_ρ	radial particle velocity
g	gravitational acceleration	$\overline{u_p}$	normalized particle axial velocity
L	distance between P_1 and P_4	$\overline{\omega_p}$	normalized particle radial velocity
Δp	pressure drop	$\overline{u_p'^2}$	particle fluctuating axial velocity
p	gage pressure	$\overline{\omega_p'^2}$	particle fluctuating radial velocity
Q_a	flow rate of gas volume	$u(t)$	given signal
S_p	sphericity	$\psi(t)$	wavelet function
T	gas temperature		

1. INTRODUCTION

Usually, air or non-reactive gases are used to convey the bulk materials in pneumatic conveying. The chief advantage of this system is its flexible layout and total containment. Owing to the limitation of conveying space, bends and the corresponding vertical tubes become the key components of the pneumatic conveying system. So far, most studies on pneumatic conveying systems have focused on horizontal pipes and bends (Li *et al*. 2021; Zhu *et al*. 2019; Kruggel-Emden and Oschmann 2014; Kalman *et al*. 2019), with a few studies focused on the motion characteristics of the particles in vertical tubes, which are an indispensable part of pneumatic conveying. Owing to this, the study of particle velocity and pressure drop in vertical tubes is essential for the overall design of the conveying systems.

Previous research on pneumatic conveying with bends concentrated on the pressure and particle flow characteristics of the bends. (Abdolkarimi and Mohammadikhah 2019; Tripathi *et al*. 2019a). Dong and Rinoshika (2019) added soft fins to the system and measured the flow velocity and particle pulsation intensity upstream and downstream of bends with varying curvature radii. The results showed that the soft fins were effective in pipes with larger *R/D*. Yan *et al.* (2021) and Tu *et al.* (2021) studied the flow characteristics of particles in different curvature radius bends by using different analysis methods to dissect the flow pattern. Yilmaz and Levy (2001) investigated the particle velocity distribution downstream of the bend and discovered that the rope structure fragmented into big discontinuous clusters. By studying the velocities of gas and particle phases, Yang and Kuan (2006) deduced the reason for particle rope production. Tripathi (2019b) analyzed the velocity reduction of vertical pipes in a pneumatic conveying system; it indicates that the particle velocity ratio increase with the increase of bending ratio, but after a certain limit, further increase in bending ratio led to a decrease in particle velocity ratio. Portnikov (2020) discovered that greater bend radius ratios produced less damage to the delivered material through experimental findings and parametric analysis. Furthermore, higher air velocities and bigger pipe diameters increased material damage. The above studies mainly analyzed the whole bend, while the flow of particles after exiting the bend into the vertical tube was less analyzed.

Dzido *et al.* (2002) studied the acceleration effect of spherical and non-spherical particles in vertical tubes for pneumatic conveying. Burazer *et al.* (2014) analyzed the effect of conveying particles of different materials in a vertical tube on the gas velocity. El-Behery *et al.* (2017) find that the particle density, solid mass flow rate, and particle size will change the MPD velocity and pressure drop in vertical tubes for pneumatic conveying. *Tripathi et al.* (2018) give an idea about the flow characteristics of particles in vertical tubes in different directions by comparing particle shape, acceleration length, and void fraction. Yang *et al.* (2019) analyzed the dynamic characteristics of large non-spherical particles in a vertical flow field based on the experimental and simulation results of particle suspension. The experimental show that the rotation of non-spherical particles in the vertical flow field can reduce the flow velocity requirement of large non-spherical particles in vertical pneumatic conveying. Azzopardi (2017) derived an equation to represent the effect of pressure on frequency; when the system consists of a horizontal pipe, a bend and a vertical tube, there is a segment plug flow in the horizontal section, and the frequency of the vertical segment plug flow can be the same as the frequency of the horizontal segment plug flow. Kuang *et al.* (2009) conducted a three-dimensional numerical study of vertical pneumatic conveying and successfully identified the dilute and dense phase flow in the vertical tube. The above studies mainly analyze the flow of particles in vertical tubes, At the same time there is no study on the flow characteristics of particles in vertical tubes corresponding to different curvature radius bends.

In this research, the dynamic properties of particles in a gas-solid two-phase flow in a vertical tube are investigated with the help of three distinct curvature radius bends and corresponding vertical tubes. In this experiment, the velocity distribution of the particles in the 90° bend and the corresponding vertical tube is measured by PIV, and the dynamic properties of particles are investigated for parameters like pressure drop, power consumption, the evolution of particle velocity, the intensity of particle fluctuation velocity, power spectrum characteristics and time-frequency characteristics of particle fluctuation velocity.

2. EXPERIMENTAL EQUIPMENT AND PROCEDURE

2.1 Equipment and Materials

The experimental equipment is depicted in Fig. 1. It comprises a control system, a feeder, filter, and a fan. In this study, the experimental pipeline is made of two horizontal pipes (L = 4000mm) and they have an inner diameter of D = 80mm ± 2.46%. As show in Fig. 2, three vertical tubes with lengths of 1780mm, 1580mm, 1380mm, and three sets of 90° bends with radius of 300mm, 400mm, and 500mm, and the radius ratio are R/D = 3.75, 5, and 6.25 respectively. On the horizontal pipe and the vertical tube, a flow meter and pressure sensors (P_1 — P_4) are fitted. P_1 is put at the particle outlet, while P_4 is fixed at outlet of

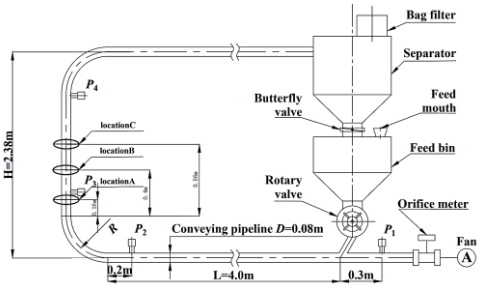

Fig. 1. Schematic diagram of the experimental apparatus.

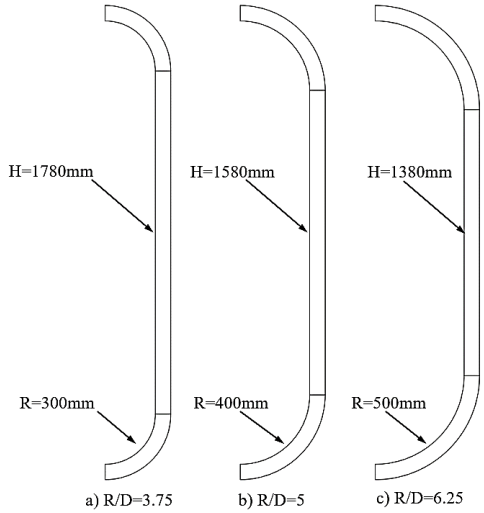

Fig. 2. Experimental bends.

the vertical tube. This experiment investigated the different particle mass flow rates are G_s = 0.25 kg/s and 0.44 kg/s, Meanwhile, the air velocity (U_a) range of the conveyed particles is from 10 m/s to 22 m/s. Ten tests are carried out under the same conditions, and the statistical uncertainty of gas density ρ_a (T ± 5.12%), G_s, gas velocity U_a , and gage pressure p in the 95% confidence level are ± 1.53%, ± 1.94%, ± 5.56% and ± 4.16%, respectively. T represents the temperature of the experimental environment.

As illustrated in Fig. 3(a), the non-spherical polyethylene particles are employed in this investigation and the particle's physical properties are the poisson ratio (μ = 0.41), particle bulk density (598 kg/m^3), elastic modulus (E = 1.12Gpa), shear elasticity (G = 3.77Gpa), bulk voidage (a = 0.357), and particle density (ρ= 953 kg/m^3).

$$d_{ep} = 2\sqrt{A_p/\pi} \quad (1)$$

Equation (1) allows the calculation of the equivalent diameter(d_{ep}) of the particles. Here A_p is the projected area of the particle. One hundred particles are randomly selected, and the equivalent diameter of them are calculated by the MATLAB. Fig. 3(b) shows the range of d_{ep} is 3.5mm~6mm, and the particles had an average equivalent diameter of 4.58mm.

2.2 Particle Velocity Measurement

The method of measuring particle velocity by high-speed PIV is shown in Fig. 4, and the motion of the particles in the vertical tube and the bend were photographed separately. To illuminate the particle flow, it uses a laser (GG532) light-sheet with b = 6mm thickness. 4000 photos are taken in 1.2 seconds by a high-speed camera (pco.dimax S1). The particle velocity distribution is measured at the bend and vertical tube, where y is the direction of axial motion of the particles and is denoted by u_p, x represents the radial direction which is corresponding to particle velocity component ω_p. θ is the remaining angle between tangent line of the outer wall of the bend and the direction of gravity.

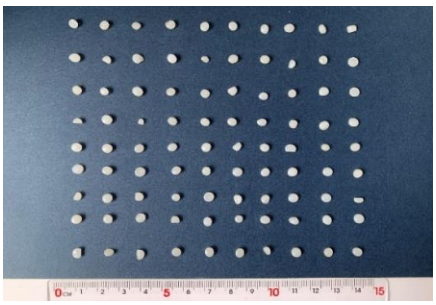

(a) Particles.

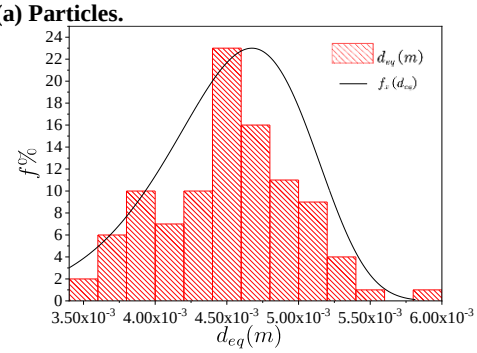

(b) Particle size and distribution.

Fig. 3. Distribution of particles with different diameters.

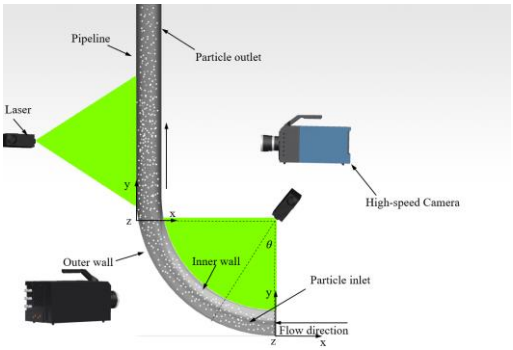

Fig. 4. High-speed PIV measurement system.

3. RESULTS AND DISCUSSION

3.1 Pressure Drop and Power Consumption

Figure 5 depicts the pressure drop(Δp) of the pneumatic conveying system by using different radius bends and conveying different quality of particles. The minimum pressure drop (MPD) velocity is defined as the lowest air velocity when carrying particles loss the lowest energy and do not result in choking.

Figure 5(a) shows the working condition of conveying particle mass of G_s = 0.25kg/s. The pressure drop first decrease to the MPD velocity and then increase as the gas velocity increasing, and MPD velocities decrease as the bend ratios increases (the MPD velocity of R/D =3.75 is 16.21m/s, for R/D = 5 is 16.1m/s and for R/D = 6.25 is 15.79m/s). The pressure drops in the low-velocity region (U_a < 12m/s) are same as three different curvature radius bends. However, Δp is decrease with the increase of curvature ratios (U_a > 12m/s).

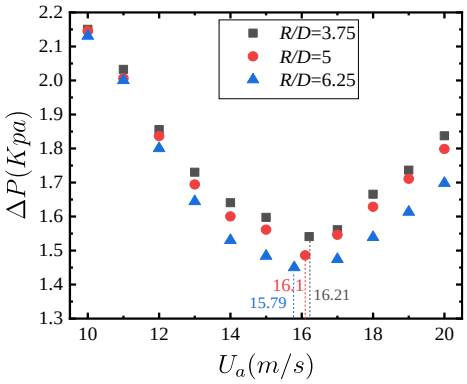

a) G_s = 0.25kg/s.

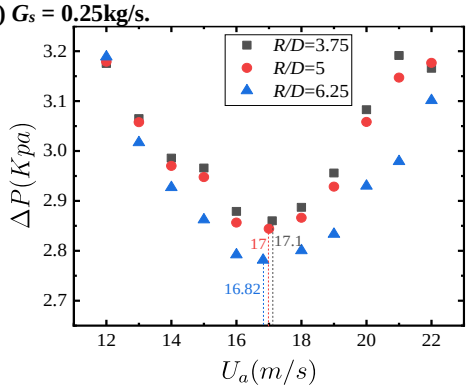

b) G_s = 0.44kg/s.

Fig. 5. Pressure drop of the system at different gas velocity for G_s = 0.25kg/s and 0.44kg/s.

Figure 5(b) plot the pressure drop of G_s = 0.44kg/s, the distribution trend of pressure drop is same as the case of G_s = 0.25kg/s but the MPD velocities increase. The velocity of *R/D* =3.75 is 17m/s, for *R/D* = 5 is 16.82m/s and for *R/D* = 6.25 is 16.21m/s.

To investigate the power consumption of different *R/D* bends, this study uses the power consumption coefficient *E* to calculate.

$$E = \frac{\Delta p Q_a}{g G_s L} \tag{2}$$

Here Δp is the pressure drop between meters P_1 to P_4, G_s is the mass flow rate of particles, Q_a is the flow rate of gas volume, L denotes the distance between P_1 and P_4, and g is the gravitational acceleration

Figure 6 shows the power consumption coefficients *E* of the system using different radius bends for different gas velocities at G_s = 0.25kg/s and 0.44kg/s. It is seen that *E* decreases and then increases with the increase of the gas superficial velocity. For the case of G_s = 0.25kg/s, *E* is same as three different radius ratios at the high gas velocity region (U_a > 17m/s) and decreases with the increase of radius ratios ($U_a \leq$ 17m/s). Otherwise, the distributions trend of *E* for the case of G_s = 0.44kg/s are similar to the case of G_s = 0.25kg/s. However, the *E* of all cases for three *R/D* bends is higher than the case of G_s = 0.25kg/s in the region of $U_a \leq$ 17m/s. The above results suggest that in a pneumatic conveying system, a large curvature radius bend is more effective for minimizing

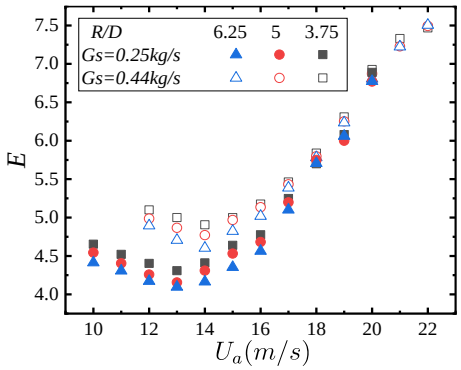

Fig. 6. Power consumption coefficient at different gas velocity for G_s = 0.25kg/s and 0.44kg/s.

pressure drop, power consumption, and conveying air velocity.

To evaluate the influence of the bend and its corresponding vertical tube on the pressure drop of the system, normalization factor D_r is proposed:

$$D_r = \frac{\Delta p_{24}}{\Delta p_{14}} \tag{3}$$

Where Δp_{24} is the pressure drop of vertical tube and bend, Δp_{14} is the pressure drop of the system.

Figure 7 shows the normalization factor D_r proportion with different *R/D* bends at G_s = 0.25kg/s and 0.44kg/s. D_r decreases with the increase of *R/D* and the D_r of G_s = 0.25 kg/s is higher than G_s = 0.44 kg/s. The range of D_r is from 35.2% to 44.1%, and the minimum D_r is 35.2% corresponds to the bend of *R/D* = 6.25. It suggests that the pressure drops in bends and vertical tubes achieve a high proportion of a horizontal-vertical pneumatic conveying system. As a result, it is vital and necessary to investigate the particle movement characteristics in the bends and their corresponding vertical tubes in this study.

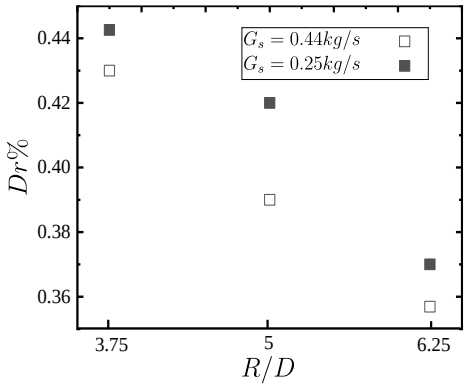

Fig. 7. Normalized pressure drop proportion with different *R/D* bends at *Gs* = 0.25kg/s and 0.44kg/s.

3.2 Flow Characteristics of Particles in the Bend

To study the flow characteristics of particles in different radius bends at G_s = 0.25kg/s and 0.44kg/s,

the particle velocities in three different *R/D* bends are measured by PIV in this study.

Figure 8 shows the axial velocity ($\overline{u_p}$ / U_a) of the particles in the bend versus θ for different *R/D* bends at G_s = 0.25kg/s and 0.44kg/s. It can be observed that the $\overline{u_p}$ / U_a decreases with the increase of θ except for $40^0 < \theta < 70^0$ at G_s = 0.25kg/s and 0.44kg/s.

For the case of G_s = 0.25kg/s, the $\overline{u_p}$ / U_a of different radius bends shows obvious fluctuates around the entrance velocity at the inlet of bend ($0^0 < \theta < 20^0$), which may be because the motion state of the particles does not change due to inertia when the particles enter the bend from the horizontal tube. Meanwhile, $\overline{u_p}$ / U_a decreases rapidly at $20^0 \leq \theta < 40^0$, the reason is that the energy exchange in the upward motion against gravity and he collision of the particles with the tube wall after entering the bend. Additionally, the reduced rate of $\overline{u_p}$ / U_a decrease as the bend radius increase and may be this is the reasons why Δp is smaller in large curvature radius bends. In the region of $40^0 \leq \theta < 60^0$, the $\overline{u_p}$ / U_a remains the same because the particles are again subjected to the action of inertia. Moreover, at the exit of the band ($60^0 \leq \theta < 90^0$) the distribution of $\overline{u_p}$ / U_a in the three different radius bends are basically the same. The above results show that a larger radius bend is more conducive to particle acceleration.

For the case of G_s = 0.44kg/s, the distribution of $\overline{u_p}$ / U_a in the bend is same as G_s = 0.25kg/s, but the value of $\overline{u_p}$ / U_a for each *R/D* is smaller than G_s = 0.25 kg/s. This may be due to the violent collision of particles with high mass flow rate in the bend and high energy loss, which is also one of the reasons why power consumption coefficients *E* of G_s = 0.44 kg/s is higher than G_s = 0.25kg/s.

As shown in Fig. 9. the relationship between three different *R/D* bends and normalized particle radial velocity ($\overline{\omega_p}$ / U_a) at G_s = 0.25kg/s and 0.44kg/s. It can be seen that the absolute value of $\overline{\omega_p}$ / U_a increase with the increase of θ at the region of $0^0 < \theta < 20^0$, this is because inertia mainly affects the motion of particles, and this is also the reason why the value of $\overline{u_p}$ / U_a do not change much at this region. However, at the region of $20^0 \leq \theta < 40^0$ the absolute value of $\overline{\omega_p}$ / U_a decrease to zero, the reason for this phenomenon is that when the particle moves to the middle of the bend, the collision of the particle-particle and the particle-wall violently, which causes the higher energy loss and reduces the velocity of the particle at this region. Furthermore, under the action of inertia again, the particle velocity increases at the region of $40^0 \leq \theta < 60^0$. At the same time, the $\overline{\omega_p}$ / U_a is lower for bend with larger radii, but the $\overline{u_p}$ / U_a is higher than others (Fig.8). At the region of $60^0 \leq \theta < 90^0$, the $\overline{\omega_p}$ / U_a decrease with the increase of θ but for the case of *R/D* = 6.25, the $\overline{\omega_p}$ / U_a increase and then decrease, it's possible that a bend with larger radii cause fewer particle-wall /particle collisions. It can also be

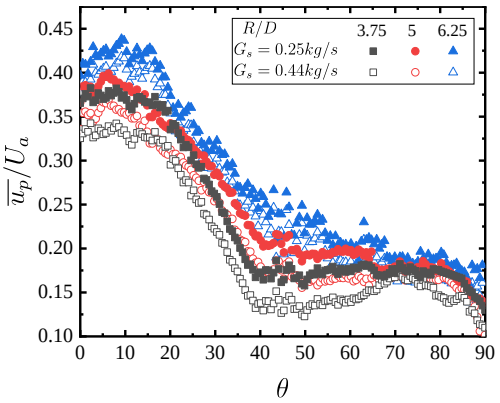

Fig. 8. Axial velocity of particles in bends of different radii.

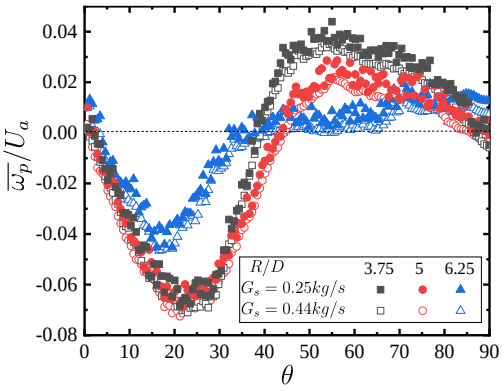

Fig. 9. Radial velocity of particles in bends of different radii.

observed from Fig. 9, the $\overline{\omega_p}$ / U_a of the particles is independent of the particle mass flow rate.

3.3 The Evolution of Particle Velocity in Vertical Tube

Figure 10 presents the flow pattern of particles coming out of the bend into the vertical tube at G_s = 0.25 kg/s. The particle flow patterns in the vertical tube are measured by high-speed PIV at MPD velocity and the measurements are performed at three different locations: *y* = 0.16 m (*y/D* = 2, location A), 0.4 m (*y/D* = 5, location B) and 0.56 m (*y/D* = 7 location C) from the inlet of the vertical tube (Fig. 1).

At location A, it can be observed that the particles mainly move along the outer wall of the vertical tube and the concentration is higher. In the vertical tube corresponding to *R/D* = 3.75, the particles gather more obviously at the outer wall, and in the vertical tube corresponding to *R/D* = 5, the particles tend to disperse toward the center of the tube. While in the vertical tube corresponding to *R/D* = 6.25, the concentration of particles in the outer wall of the tube is smaller than in the remaining two tubes, and the dispersion of particles in the tube is better. It indicates that the bend with larger curvature radius is benefit for particle dispersion when the particles enter the vertical tube.

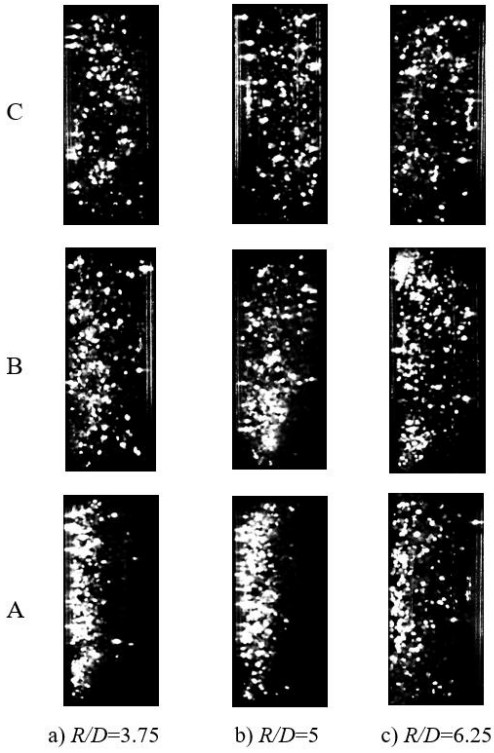

Fig. 10. PIV images of particle flow pattern at three different locations for G_s = 0.25kg/s.

At location B, the particles are more dispersed than location A. However, the distribution of particles in the vertical tube corresponding to *R/D* = 6.25 are more dispersed. Moreover, there is no significant difference in the dispersion effect of the particles in the three vertical tubes when the particles move to the stable location C. The particles in these three tubes are uniformly distributed.

3.3.1 Axial Velocity of Particles in Vertical Tube

Figure 11 shows the profiles of the time-averaged axial component ($\overline{u_p} / U_a$) of particle velocity for three different locations at G_s = 0.25kg/s and 0.44 kg/s.

At location A, as shown in Fig. 11(a), the $\overline{u_p} / U_a$ of the particles gradually increases from the outer wall to the inner wall of the tube at G_s = 0.25kg/s. This is because the higher concentration of particles at the outer wall of the vertical tube leads to significant collisions. In comparison the lower concentration of particles near the inner wall of the vertical tube results in greater $\overline{u_p} / U_a$ under the action of air. At the same time, the $\overline{u_p} / U_a$ of the particles increases sequentially in the vertical tube, corresponding to *R/D* = 3.75, 5, and 6.25. It is probably due to the collision of particle-to-particle/tube wall decreases with the increase of the curvature radius thus, the energy loss is less. Meanwhile, the distribution of $\overline{u_p} / U_a$ for the case of G_s = 0.44kg/s is same as G_s = 0.25kg/s, but the values of $\overline{u_p} / U_a$ are smaller than G_s = 0.25kg/s, which indicates the larger particle mass flow rate will cause the significant particle

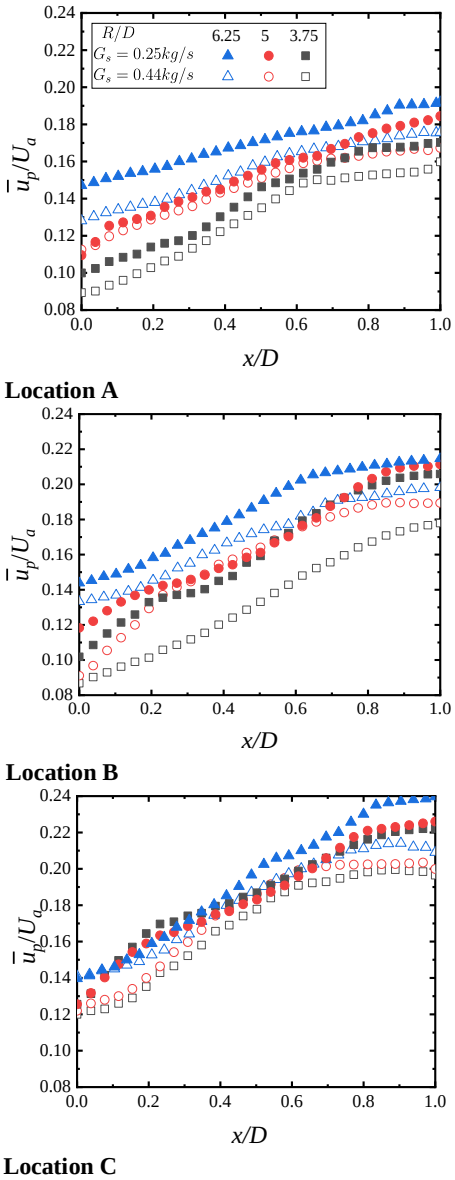

Fig. 11. Axial velocity distribution at three locations in the vertical tube.

collisions, and the greater energy loss resulting in a small $\overline{u_p} / U_a$ in the vertical tube.

At location B (Fig. 11b), under the action of inertia, the distributions of $\overline{u_p} / U_a$ in the outer wall of the vertical tube are basically unchanged compared with location A, while the $\overline{u_p} / U_a$ in the inner wall of the vertical tube is greater than location A, what indicating that the particles start to accelerate at location B for G_s = 0.25kg/s and G_s = 0.44kg/s. At location C, as shown in Fig. 11(c), the distribution of $\overline{u_p} / U_a$ in the vertical tubes corresponding to different *R/D* bends is essentially the same except for *R/D* = 6.25 in the region of 0.4 < *x* /*D* < 1 at G_s = 0.25kg/s. The reason for this phenomenon is that as the conveying height increases, the particles are completely dispersed in the vertical tubes corresponding to three different curvature radius bends under the effect of inertia. In contrast the

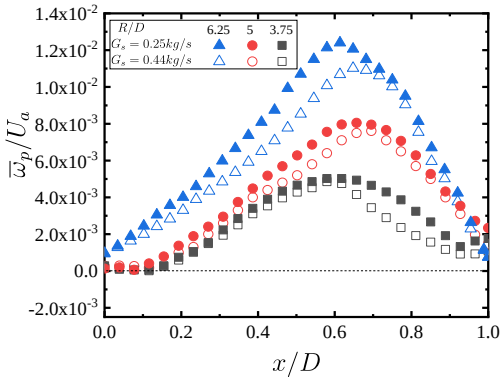

a) Location A

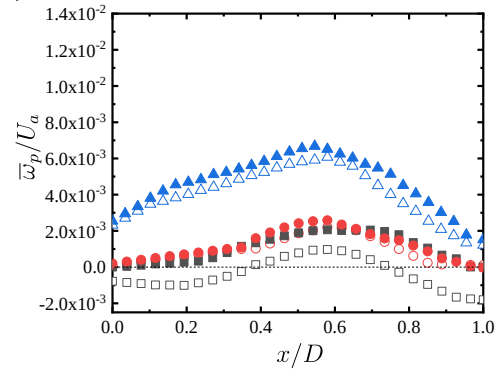

b) Location B

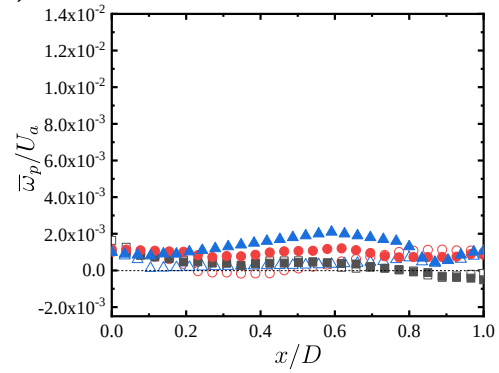

c) Location C

Fig. 12. Radial velocity distribution at three locations in the vertical tube.

particles have a longer acceleration distance in the large curvature radius bend, which makes the particles have a higher velocity in its corresponding vertical tube.

3.3.2 Radial Velocity of Particles in Vertical Tube

Figure 12 shows the profiles of normalized time-averaged particle radial velocity $\overline{\omega}_p / U_a$ in the vertical tube for three different locations at G_s = 0.25kg/s and 0.44kg/s. At location A, as indicated in Fig. 12(a), the $\overline{\omega}_p / U_a$ of particles in the vertical tube corresponding to different radius bends is positive for G_s = 0.25kg/s, and the $\overline{\omega}_p / U_a$ increases and then decreases from the outer wall to the inner wall of the vertical tube. Whereas $\overline{\omega}_p / U_a$ reach the peak near *x/D* = 0.6, this is because most of particles in the center of the tube move mainly towards the inner wall under the action of inertia. Meanwhile, the $\overline{\omega}_p / U_a$ in the vertical tube corresponding to *R/D* = 6.25 is larger than the $\overline{\omega}_p / U_a$ in the vertical tube corresponding to *R/D* = 5 and 3.75. This suggests that the particles are fully suspended in the vertical tube corresponding to the large curvature radius bend, it is another important reason why a large curvature radius bend can reduce pressure drop and minimum air velocity. For the case of G_s = 0.44kg/s the trend of $\overline{\omega}_p / U_a$ is same as G_s = 0.25kg/s, but the value is smaller than G_s = 0.25kg/s.

At location B, as indicated in Fig. 12(b), the value of $\overline{\omega}_p / U_a$ for all cases is smaller than location A, for the case of G_s = 0.44kg/s the $\overline{\omega}_p / U_a$ of *R/D* = 3.75 is negative at the region of 0 < *x/D* < 0.4 and 0.7 < *x/D* < 1. This is because the particles collide with the tube wall resulting in opposite directions of motion. Additionally, the $\overline{\omega}_p / U_a$ of particles in the vertical tube corresponding to *R/D* = 6.25 is still larger than the $\overline{\omega}_p / U_a$ of particles in the vertical tube corresponding to *R/D* = 5 and 3.75.

As indicated in Fig. 12(c), with the conveying hight increase the $\overline{\omega}_p / U_a$ reduces close to zero in the vertical tube corresponding to three different *R/D* bends at G_s = 0.25kg/s and G_s = 0.44kg/s. This is because the particles arrive at the stable location C with mainly axial motion, and radial motion does not dominate.

3.4 The Intensity of Particle Fluctuation Velocity in Vertical Tube

To evaluate the fluctuating energy of the particle velocity in the vertical tube, the velocity fluctuations ($\overline{u_p'^2}$ and $\overline{\omega_p'^2}$) of particles are calculated. The statistical uncertainties of $\overline{u_p'^2}$ and $\overline{\omega_p'^2}$ are ± 3.59% and ± 0.63% at the 95% confidence level, respectively. Fig. 13 and Fig. 14 show the intensity of particle fluctuation velocity $\overline{u_p'^2}/u_a^2$ and $\overline{\omega_p'^2}/u_a^2$ at G_s = 0.25kg/s and 0.44*kg/s* for three different locations of the vertical tube corresponding to different radius bends.

Figure 13(a) plots the profiles of $\overline{u_p'^2}/u_a^2$ at location A, the $\overline{u_p'^2}/u_a^2$ decreases and then increases from the outer wall to the inner wall of the vertical tube. The $\overline{u_p'^2}/u_a^2$ in the vertical tube corresponding to *R/D* = 6.25 is higher than the $\overline{u_p'^2}/u_a^2$ in the vertical tubes corresponding to *R/D* = 5 and 3.75. For the case of G_s = 0.25kg/s, the $\overline{u_p'^2}/u_a^2$ is not heavy at the region of 0 < *x/D* < 0.6. It's because the particle concentration is larger closer the vertical tube's outer wall, which results in smaller velocity fluctuations. Meanwhile, at 0.6 < *x/D* < 1, the span of $\overline{u_p'^2}/u_a^2$ for larger radii bend is higher. This indicates that a considerable fluctuating energy of particle velocity in the suspension flows, and the particles are more active in the inner wall of the vertical tube corresponding to large curvature radius bends.

For the case of G_s = 0.44kg/s, the distribution of $\overline{u_p'^2}/u_a^2$ is the same as G_s = 0.25kg/s, but the value is

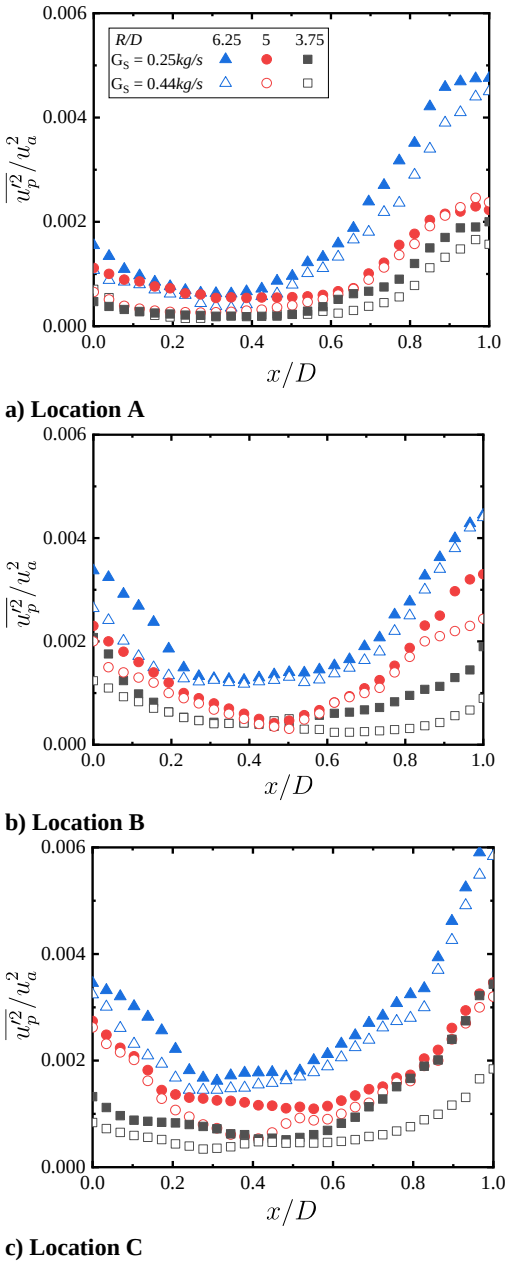

Fig. 13. Intensity of particle fluctuation velocity $\overline{u_p'^2}/u_a^2$ at three different locations for different *R/D* bends.

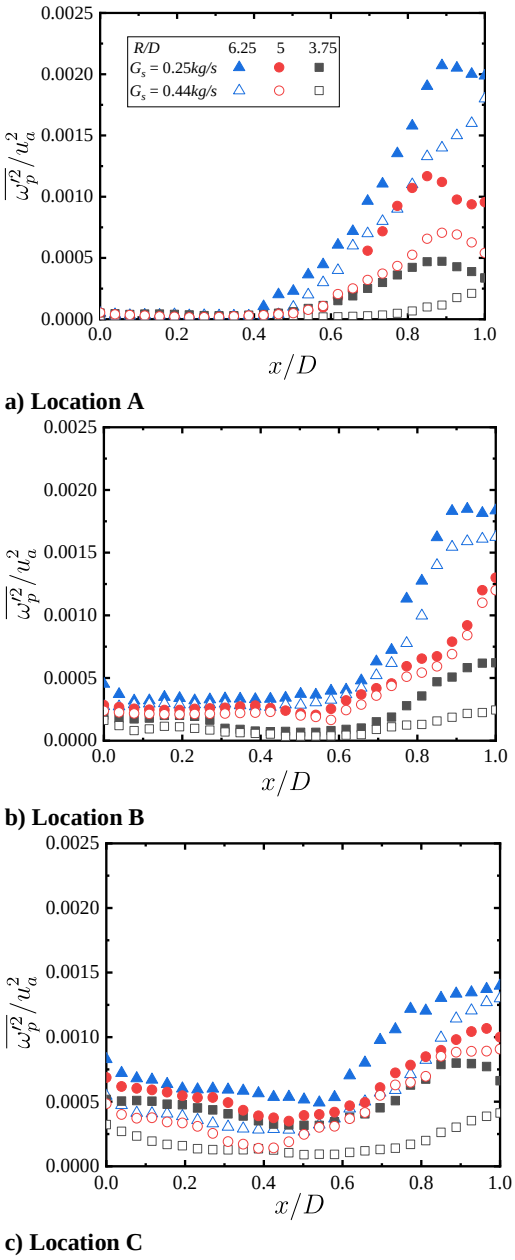

Fig. 14. Intensity of particle fluctuation velocity $\overline{\omega_p'^2}/u_a^2$ at three different locations for different *R/D* bends.

small. This could be because the pressure gradient rises as the particle mass flow rate rises, and the higher the pressure gradient, the more prominent the particle rope, which reduces the particle fluctuation velocity in the tube.

At location B as shown in Fig. 13(b), the $\overline{u_p'^2}/u_a^2$ in the outer wall of the vertical tube is significantly larger than in location A, which means that the accumulation of particles on the outer wall of the vertical tube has a reduced effect on the fluctuation of particles. The $\overline{u_p'^2}/u_a^2$ increases with increasing conveying distance near the inter wall of the vertical tube (Fig. 13c), and the fluctuation intensity of particles in the vertical tube corresponding to *R/D* = 6.25 remains higher than those corresponding to *R/D* = 5 and 3.75. It implies that the particles are completely dispersed at location C and they move in large curvature radius bends that are more conducive, and the higher $\overline{u_p'^2}/u_a^2$ is also the reason for the particles in the vertical tube corresponding to large curvature radius bends has a maximum $\overline{u_p}$ / U_a at location C.

Figure 14 shows the intensity of the radial fluctuation velocity of the particles in the vertical tube. It can be observed in Fig. 14(a), that the $\overline{\omega_p'^2}/u_a^2$ is almost to zero at 0 < *x/D* < 0.4, which is caused by the aggregation of particles at this location. The growth rate of $\overline{\omega_p'^2}/u_a^2$ for *R/D* = 6.25 at 0.4 < *x/D* < 1 is

greater than *R/D* = 5 and 3.75, this indicating that the particles are more likely to be suspended in the vertical tube, corresponding to a large curvature radius bends. As the conveying distance increases (Fig. 14b), the $\overline{\omega_p'^2}/u_a^2$ is greater than location A near outer wall of the vertical tube, which indicates that the particles begin to disperse under the drive of air. At location C, as shown in Fig.14(c), the maximum of $\overline{\omega_p'^2}/u_a^2$ is smaller than in other locations, it means that the particles are completely dispersed at this location, most of them move mainly upward, and the radial fluctuations are converted to axial fluctuations.

3.5 Power Spectra of Axial Particle Fluctuating Velocity in Vertical Tube

The purpose of this research is to look at the variable velocity characteristics of particles at three different locations along the vertical tube, the particle fluctuating velocities at *y/D* = 2, 5 and 7 at the MPD velocity are calculated using the Fourier transform and tested using a high-speed PIV. The power spectral density function *P* is defined as $\int_{-\infty}^{+\infty} P\,df = \overline{u_p'^2}$, and frequency *f* is normalized by $\overline{u_p'^2}$ to show the energy distribution in its normalized form.

Figure 15 depicts the power spectrum of particle fluctuation velocity and frequency distribution of the particle fluctuation kinetic energy for three vertical tubes corresponding to different *R/D* bends at G_s = 0.25kg/s. Exhibit peaks of $p/\overline{u_p'^2}$ increase with the increasing of *R/D*, as seen in Fig.15(a), and the value of $p/\overline{u_p'^2}$ is larger than in other areas. Simultaneously, the prominent peaks of $p/\overline{u_p'^2}$ are mostly dispersed in the low-frequency range, and the peak of $p/\overline{u_p'^2}$ declines as frequency increases. This may be due to the particle concentration being greater and most of them accumulating on the tube's outer wall when the particles flow from the bend to the vertical tube (Yan and Rinoshika2013).

At *y/D* = 5, as illustrated in Fig. 15(b), the distributions of the power spectrum are the same as in Fig. 15(a), whereas the pronounced peaks of $p/\overline{u_p'^2}$ are smaller than *y/D* = 2. For the fully developed regime of *y/D* = 7 (Fig. 15 c), the value of $p/\overline{u_p'^2}$ becomes smaller than *y/D* = 2 and 5. Moreover, the power spectrum's peaks can still be seen in the low frequency region, and the peaks of $p/\overline{u_p'^2}$ for vertical tube with larger radii bend are still higher than the vertical tube with small radii bend

The above results manifest that the particles are better accelerated in the vertical tube corresponding to a large curvature radius bend, which leading to a more intense flow of particles and causes larger fluctuation energy.

3.6 Time-frequency Characteristics of Particle Fluctuation Velocity

To further reveal the dynamic characteristics of particles in vertical tubes corresponding to different curvature radius bends, the continuous wavelet transform (CWT) is used to perform time-frequency analysis of the fluctuating velocity of particles in the

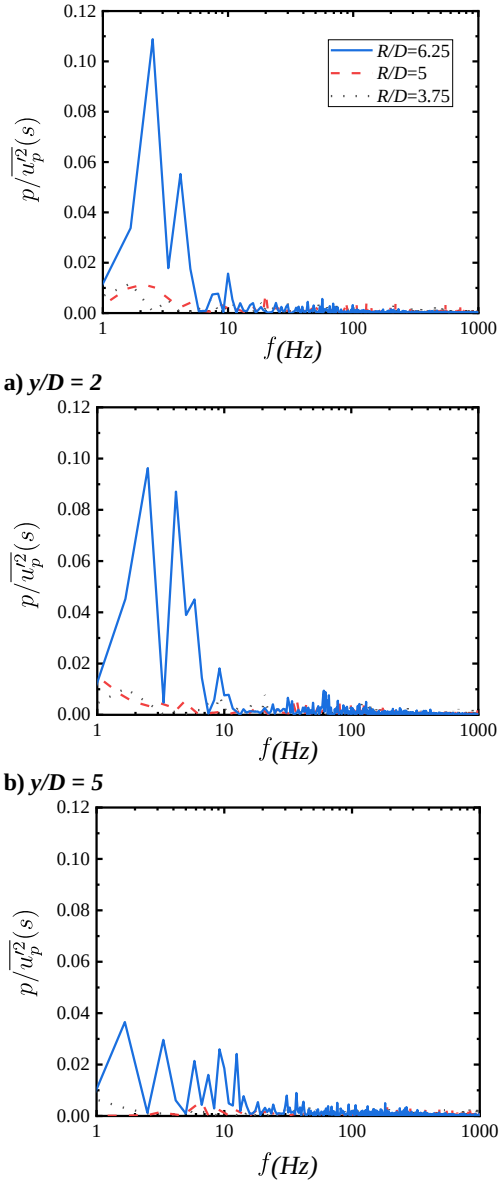

Fig. 15. Power spectra of axial particle fluctuating velocity near *x/D* = 0.25 at three different locations for different *R/D* bends (G_s = 0.25kg/s).

tube. The continuous wavelet transform is used to divide the signal into many small time intervals, and each time interval is analyzed by Fourier transform to determine the frequency present at that time interval. The CWT is defined as the convolution operation between a given signal $u(t)$ and the wavelet function $\psi(t)$, and the formula below is used to calculate it:

$$Wf(\tau,s) = \frac{1}{s}\int_{-\infty}^{+\infty} u(t)\psi^*\left(\frac{t-\tau}{s}\right)dt \quad (4)$$

Where $Wf(\tau,s)$ is called the wavelet coefficient at translation τ and scale s in the time-scale plane, * stands for complex conjugate, $\psi(t)$ is the mother wavelet function and wavelet function at translation

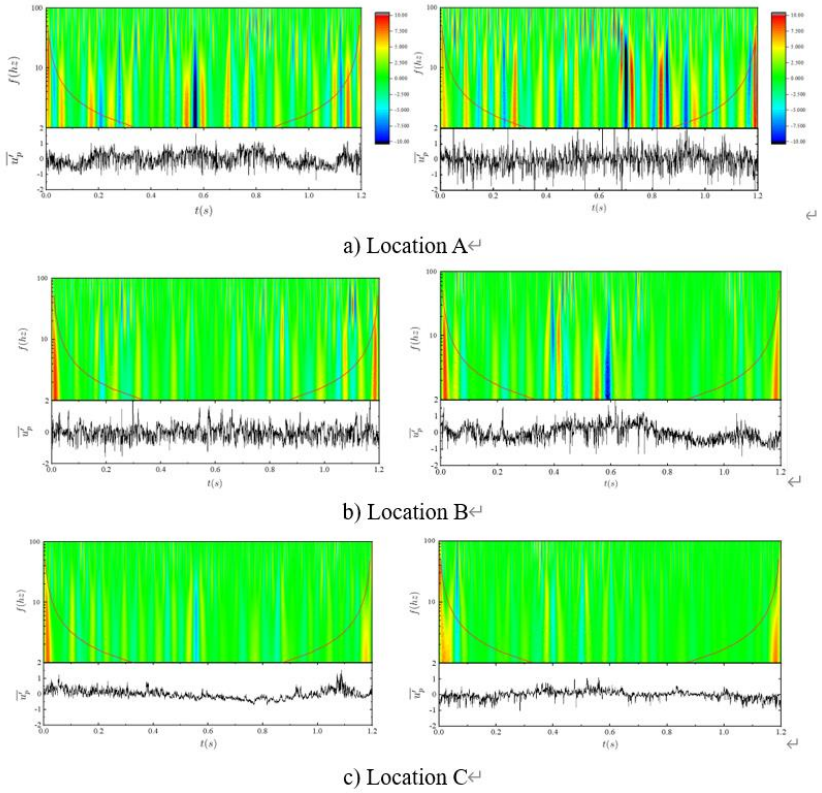

Fig. 16. Time-frequency distributions of the axial fluctuation velocity for three different locations with the bend of *R/D* = 3.75 (left) and *R/D* = 6.25 (right).

τ and scale s is indicated by $\psi^*\left(\frac{t-\tau}{s}\right)$. In this study, the Mexican hat wavelet is applied to the particle fluctuation velocity in the measurement domain, and it is defined as:

$$\psi\left(\frac{t-\tau}{s}\right) = \left(1-\left(\frac{t-\tau}{s}\right)^2\right) e^{-\frac{1}{2}\left((t-\tau)/s\right)^2} \tag{5}$$

The scale parameter s controls the mother wavelet's contraction and expansion, as well as its frequency and window length. The wavelet's velocity along the time axis is controlled by the translation parameter τ. The contours of wavelet coefficients are shown versus time and scale (frequency) axes in the continuous wavelet transform result, which is commonly given as a cloud map.

The results of the continuous wavelet transform are shown in Fig. 16, where the colors correspond to the values of the wavelet coefficients, with the lowest concentration in blue and the highest concentration in red. The average axial velocity fluctuations are plotted below the time frequency plane versus time t.

Figure16 shows the time-frequency characteristics of the particle pulsation velocity within the three different locations of the vertical tube corresponding to the bend of *R/D* = 3.75 (left) and *R/D* = 6.25 (right). It is clear to see that from location A to location C, the peak frequency of the alternating particle axial fluctuation velocity decreases. At location A, a series of perceptible positive and negative peaks can be observed from the low-frequency region, and the alternating peak of *R/D* = 6.25 is significantly higher than that of *R/D* = 3.75, this shows that the low-frequency component of the particle axial fluctuation velocity has the upper hand, which is also the reason why the peaks of $p/\overline{u_p'^2}$ in the vertical tube corresponding to *R/D* = 6.25 are more pronounced and the greater dispersion effect of the particle in the vertical tube corresponding to large curvature radius bend.

At location B, the frequency of the alternating peak of the particle axial fluctuation velocity is smaller than that of location A. The width of the strip becomes narrower in the low-frequency region, which indicates that there is a tendency for the large-scale motion change to the small-scale motion as the conveying distance increases. When the particle reaches at stable location C, the axial velocity fluctuation is reduced which can be observed from the above Fig. 10.

The above results show that when particles enter the vertical tube from the bend, the axial velocity fluctuation is dominated by large-scale motion in the low-frequency region. In contrast, the small-scale motion dominates the high-frequency area and the axial fluctuation velocity of particles in the vertical tube corresponding to the bend with large radius bend is greater than small radius bend. As the conveying distance increases, the fluctuation of particles in the vertical tube decreases, and the fluctuation of particles in the vertical tube corresponding to different curvature radius bends in the low-frequency and high-frequency regions is no significant difference.

4. CONCLUSION

In order to study the flow characteristics of particles in vertical tubes and bends of different radii, the velocities of particles of different masses were measured at MPD velocities with high-speed PIV, and the following conclusions were obtained:

(1) The system's pressure drop decreases as the bend radius increases at different particle mass flow rates, especially *R/D* = 6.25 has a lower pressure drop and power consumption.

(2) The $\overline{u_p} / U_a$ in the vertical tubes corresponding to different *R/D* bends increases with the increase of the conveying distance. At the same time, the $\overline{\omega_p} / U_a$ decreases with the increase of the conveying distance. The $\overline{u_p} / U_a$ and $\overline{\omega_p} / U_a$ in the vertical tube corresponding to *R/D* = 6.25 are larger than the vertical tube corresponding to *R/D* = 5 and 3.75.

(3) The $\overline{u_p'^2}/u_a^2$ and $\overline{\omega_p'^2}/u_a^2$ in the inner wall of the vertical tube are higher than that of the outer wall, and the $\overline{u_p'^2}/u_a^2$ increases with the increase of conveying distance. In contrast the $\overline{\omega_p'^2}/u_a^2$ in the inner wall of the vertical tube decreases with the increase of conveying distance, and the values of $\overline{u_p'^2}/u_a^2$ and $\overline{\omega_p'^2}/u_a^2$ in the vertical tube corresponding to *R/D* = 6.25 are higher than *R/D* = 5 and *R/D* = 3.75.

(4) Larger radius bends provide a large power spectrum of particle fluctuation velocity in the low-frequency region, which is connected to pressure drop decrease. This efficiency is especially noticeable when particles enter the vertical tube from the bend.

(5) At the inlet of the vertical tube, the axial velocity of particles in the vertical tube corresponding to *R/D* = 6.25 fluctuates widely. At the same time there is no significant difference in particle fluctuation velocity in the vertical tube corresponding to different curvature radius bends as the conveying distance increases.

ACKNOWLEDGEMENTS

The author wishes to acknowledge the support given to him by the Natural Science Foundation of Jiangsu Province of China (No.BK20191459), Postgraduate Research & Practice Innovation Program of Jiangsu Province of China (KYCX21_3443).

REFERENCES

Abdolkarimi V. and R. Mohammadikhah (2013). CFD Modeling of Particulates Erosive Effect on a Commercial Scale Pipeline Bend. *ISRN Chemical Engineering*, 1–10.

Azzopardi, B. J. (2017). The frequency of periodic structures in vertical pneumatic conveying of large particles. *Chemical Engineering Science* 162, 203–208.

Burazer, J., M. Lecic and M. Dobrnjac (2014). Parametric analysis of vertical pneumatic conveying system performance. *ANNALS of Faculty Engineering Hunedoara – International Journal of Engineering*. 23–29.

Dong, L. and A. Rinoshika (2019). Self-excited pneumatic conveying through vertical curved 90° bends. *Powder Technology* 346, 291–300.

Dzido, G., M. Palica and J. Raczek (2002). Investigations of the acceleration region in the vertical pneumatic conveying. *Powder Technology* 127, 99–106.

El-Behery, S. M., A. A. El-Haroun and M. R. Abuhegazy (2017). Prediction of pressure drop in vertical pneumatic conveyors. *Journal of Applied Fluid Mechanics* 10, 519–527.

Kalman. H., N. Santo and N. M. Tripathi (2019). Particle velocity reduction in horizontal-horizontal bends of dilute phase pneumatic conveying. *Powder Technology* 356, 808–817.

Kruggel-Emden, H. and T. Oschmann (2014). Numerical study of rope formation and dispersion of non-spherical particles during pneumatic conveying in a pipe bend. *Powder Technology* 268, 219–236.

Kuang, S. B., A. B. Yu and Z. S. Zou (2009). Flow regimes in vertical pneumatic conveying. *Industrial & engineering chemistry research* 1145, 1005–1008.

Li, X., F. Yan, P. P. Tu, Y. Chen, Y. Zheng and R. Zhu (2021). Particle dynamics analysis in bend in a horizontal-vertical pneumatic conveying system with oscillatory flow. *Advanced Powder Technology* 32, 637–645.

Portnikov, D., N. Santo and H. Kalman (2020). Simplified model for particle collision related to attrition in pneumatic conveying. *Advanced Powder Technology* 31, 359–369.

Tripathi N. M., N. Santo, H. Kalman and A. Levy (2018). Experimental analysis of particle velocity and acceleration in vertical dilute phase pneumatic conveying. *Powder Technology* 330, 239–251.

Tripathi, N. M., N. Santo, A. Levy and H. Kalman (2019a). Experimental analysis of velocity reduction in bends related to vertical pipes in dilute phase pneumatic conveying. *Powder Technology* 345, 190–202.

Tripathi. N. M., D. Portnikov, A. Levy and H. Kalman (2019b). Bend pressure drop in horizontal and vertical dilute phase pneumatic conveying systems. *Chemical Engineering Science* 209, 115228.

Tu, P. P., Y. Shao, Q. Chen, F. Yan and P. Liu (2021). Multi-scale analysis on particle dynamic of vertical curved 90° bend in a horizontal-vertical pneumatic conveying system. *Advanced Powder Technology* 32, 3136–3148.

Yan, F. and A. Rinoshika (2013). High-speed PIV measurement of particle velocity near the minimum air velocity in a horizontal self-excited pneumatic conveying of using soft fins. *Experimental Thermal and Fluid Science* 44, 534–543.

Yan, F., P. P. Tu, X. Li, Y. Chen, Y. Zheng and R. Zhu (2021). Dynamic analysis of particles in vertical curved 90° bends of a horizontal-vertical pneumatic conveying system based on POD and wavelet transform. *Advanced Powder Technology* 32, 1399–1409.

Yang, D., B. Xing, J. Li, Y. Wang, N. Hu and S. Jiang (2019). Experiment and simulation analysis of the suspension behavior of large (5–30 mm) nonspherical particles in vertical pneumatic conveying. *Powder Technology* 354, 442–455.

Yang, W. and B. Kuan (2006). Experimental investigation of dilute turbulent particulate flow inside a curved 90° bend. *Chemical Engineering Science* 61, 3593–3601.

Yilmaz, A. and E. K. Levy (2001). Formation and dispersion of ropes in pneumatic. *Powder Technology* 114(1-3), 168-185.

Zhu, R., C. Luo, X. Li and F. Yan (2019). Experimental Quantification of Local Pressure Loss at a 90° Bend in Low-Pressure Dilute-Phase Pneumatic Conveying of Coarse Particles. *International Journal of Chemical Engineering*.